Adaptive beamforming for photoacoustic imaging

Suhyun Park, Andrei B. Karpiouk, Salavat R. Aglyamov, and Stanislav Y. Emelianov*

Department of Biomedical Engineering, University of Texas at Austin, Austin, Texas 78712, USA
**Corresponding author: emelian@mail.utexas.edu*

Received February 4, 2008; revised April 19, 2008; accepted April 30, 2008;
posted May 6, 2008 (Doc. ID 92438); published June 4, 2008

An adaptive photoacoustic image reconstruction technique that combines coherence factor (CF) weighting and the minimum variance (MV) method is introduced. The backprojection method is widely used to reconstruct photoacoustic tomography images. Owing to the scattering of light, the quality of the photoacoustic imaging can be degraded. CF, an adaptive weighting technique, is known to improve the lateral resolution of photoacoustic images. In addition, an MV adaptive beamforming method can further improve the image quality by suppressing signals from off-axis directions. Experimental studies are performed to quantify the spatial resolution and contrast of the adaptive photoacoustic beamforming methods. © 2008 Optical Society of America

OCIS codes: 170.5120, 100.3010, 110.3010, 110.5120.

When photoacoustic signals are detected using an array-based transducer for subsequent use in a limited-view-angle tomography, such as B-scan imaging, the backprojection method can be implemented based on delay-and-sum (DAS) ultrasound beamforming [1,2]. In the presence of light scattering and acoustic velocity inhomogeneities or phase aberrations, the spatial resolution and contrast of the photoacoustic images can be degraded. An adaptive weighting method, such as the coherence factor (CF) technique, has been shown to significantly improve the image quality in ultrasound and photoacoustic imaging [3,4]. In addition, photoacoustic images can be further improved by applying beamforming techniques developed in ultrasound imaging.

In ultrasound imaging, Gaussian, Hanning, or Hamming apodization (i.e., aperture weighting) is commonly used to reduce sidelobes, yet this broadens the mainlobe [5]. In other words, resolution is sacrificed to decrease artifacts and increase contrast. Since photoacoustic imaging is based on a one-way propagation of the response, the general apodization is not as beneficial as in ultrasound imaging [6]. Instead of utilizing the general aperture weighting, further enhancement of the image quality can be achieved by applying the minimum variance (MV) adaptive method. In this method, the optimal aperture weights are employed to minimize the variance of each dynamic receive focus [7–9]. The MV method has mostly been studied in narrowband ultrasound applications, but it can be applied to broadband imaging with dynamic prefocusing and spatial smoothing [7,9]. By suppressing signals from off-axis directions, the MV method can decrease the sidelobes and also reduce the mainlobe width.

In this Letter, a photoacoustic image formation technique based on DAS beamforming with adaptive weighting and apodization methods is introduced. Experiments were performed to analyze the spatial resolution and contrast using a phantom with point targets and a phantom with an inclusion inside, respectively. It is demonstrated that CF weighting with an MV adaptive method improves the quality of photoacoustic images.

In the backprojection or DAS beamforming method, received signals are dynamically focused to form an image. Assuming that we have an array of M elements, the prefocused and aligned signals based on delays from each element at reconstruction time t are given by $X(t)=[x_1(t)\cdots x_M(t)]^H$ (X:$M\times 1$ matrix; H denotes the conjugate transpose). The output of the beamformer $b(t)$ can be expressed as a weighted sum of the prefocused data:

$$b(t)=\sum_{m=0}^{M-1} w_m(t)x_m(t)=W(t)^H X(t), \tag{1}$$

where w_m is the aperture weight for the transducer element m and $W(t)=[w_1(t)\cdots w_M(t)]^H$ (W:$M\times 1$ matrix). If $W=[1\ 1\ \cdots\ 1]^T$ (T denotes the transpose), Eq. (1) represents a simple DAS beamforming. To find the normalized optimal aperture weights that suppress noise and off-axis signals, the MV beamformer [7,9] seeks to minimize the power of the beamformed signal that is $E[|b(t)|^2]$ while maintaining unit gain in the focal point. It is mathematically expressed as

$$\min_W W(t)^H R(t) W(t),$$

subject to

$$W(t)^H a=1, \tag{2}$$

where a ($M\times 1$ matrix) is the steering vector, which contains the time delays that focus in a specific direction, and R ($M\times M$ matrix) is the covariance matrix expressed as $R(t)=E[X(t)X(t)^H]$ assuming $E[X(t)]=0$. The solution (W_{MV}:$M\times 1$ matrix, optimal aperture weights) of Eq. (2) by the Lagrangian multiplier theory [8] is

$$W_{\mathrm{MV}}(t)=\frac{R(t)^{-1}a}{a^H R(t)^{-1}a}. \tag{3}$$

Since X was acquired by applying the appropriate delays on each of the received signals to focus the signals in a specific direction, Eq. (3) can be computed with the steering vector $a=[1\ 1\ \cdots\ 1]^T$. To ob-

0146-9592/08/121291-3/$15.00

tain a good estimate of the covariance matrix, spatial smoothing in which the array was divided into $M-L+1$ overlapping subgroups was utilized [7,9]. Then, the estimated covariance matrix R_{SS} ($L \times L$ matrix) becomes

$$R_{SS}(t) = \frac{1}{M-L+1} \sum_{l=0}^{M-L} X_l(t) X_l(t)^H, \tag{4}$$

where L is the number of subarray elements and $X_l(t) = [x_l(t) x_{l+1}(t) \cdots x_{l+L-1}(t)]^H$ (X_l: $L \times 1$ matrix). The parameter R_{SS} from Eq. (4) replaces R in Eq. (3). After the optimal aperture weights (W_{MV-SS}: $L \times 1$ matrix) were computed, we obtained the final beamformed output from the MV adaptive method as

$$b_{MV}(t) = \frac{1}{M-L+1} \sum_{l=0}^{M-L} W_{MV-SS}(t)^H X_l(t). \tag{5}$$

With the MV adaptive method, the signal coherence can also be adaptively considered, which is known as the CF [3,4]. The CF is defined as

$$\mathrm{CF}(t) = \frac{\left| \sum_{m=0}^{M-1} x_m(t) \right|^2}{M \sum_{m=0}^{M-1} |x_m(t)|^2}. \tag{6}$$

Thus, the beamforming equation, which combines the MV adaptive method and the CF weighting is

$$b_{MV+CF}(t) = \frac{\mathrm{CF}(t)}{M-L+1} \sum_{l=0}^{M-L} W_{MV-SS}(t)^H X_l(t). \tag{7}$$

Experiments were performed to show the spatial resolution and contrast of the photoacoustic images reconstructed using the adaptive weighting and apodization methods. The first set of experiments was conducted using a phantom with point targets. Four 250 μm diameter blue nylon strings, orthogonally oriented to the imaging plane and representing point targets, were placed in a 20% milk solution (reduced scattering coefficient, 5 cm^{-1}; absorption coefficient, 0.005 cm^{-1}) [10]. The point targets were positioned along the vertical axis every 10 mm with the first point target located 3 mm away from the transducer surface. For studies of image contrast, a phantom with an inclusion was constructed. The phantom contained 6% of porcine gelatin mixed with 1% of amberlite in the background. The 10 mm diameter circular inclusion was made out of 12% porcine gelatin, 1% amberlite, and 0.01% graphite (absorption coefficient, 3.17 cm^{-1}). The amberlite particles were acting as the light scatterers, and the graphite flakes were used as optical absorbers. The inclusion was positioned in the center of the phantom so that the center of the inclusion was 25 mm away from the transducer.

A cortex ultrasound imaging system (Winprobe Corporation, North Palm Beach, Florida) was used for rf data acquisition. This ultrasound imaging system was interfaced with a 7 MHz center frequency, 14 mm wide, and 128 element linear array transducer to image the point sources and with a 5 MHz center frequency, 38 mm wide, and 128 element linear array transducer to image the inclusion phantom. The imaging system was connected to an optical parametric oscillator laser system (7 ns pulse duration, 10 Hz repetition rate, and 12.5 $\mathrm{mJ/cm}^2$ fluence at 720 nm in wavelength). To image the phantom with point sources, the transducer was always positioned at the top, while the laser was delivered from the top in the case of the phantom with point sources and from the bottom in the case of the phantom with an inclusion. After photoacoustic data were acquired, reconstruction was performed using a simple DAS beamforming method [Eq. (1)], DAS with the MV adaptive method [Eq. (5)], DAS with CF weighting [3], and DAS with both CF weighting and the MV adaptive method [Eq. (7)]. In the MV adaptive methods, subarray elements $L=60$ and $L=32$ were chosen to employ the optimal weights for point targets and the inclusion phantom, correspondingly [9].

The photoacoustic images of the phantom with four point sources, Figs. 1(a)–1(d), were reconstructed using the simple DAS method, DAS with the MV method, DAS with CF weighting, and DAS with CF weighting and the MV method, respectively. These beamformed images, measuring 14 mm laterally and 40 mm axially, are displayed using a 35 dB log-scale dynamic range. Although the MV method [Fig. 1(b)] helps to reduce the beamforming artifacts, the CF weighting drastically improves the image in Fig. 1(c). In a combined MV adaptive method and CF weighting [Fig. 1(d)], the lateral resolution is further improved.

In general, the spatial resolution is determined by the minimal distance between two resolvable points. However, using numerical analysis [2], we confirmed that the resolution of our beamforming approach can be evaluated from the width of the mainlobe obtained from a single point source. To quantitatively analyze the lateral resolution, the lateral profiles of the point spread function (PSF) at 3 and 23 mm depths are presented in Fig. 2. Clearly, the CF weighting re-

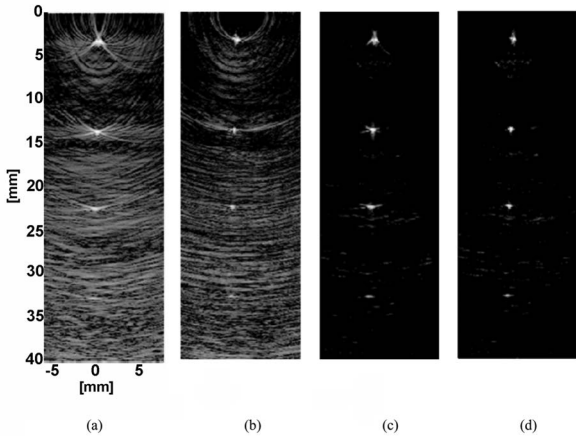

Fig. 1. Reconstructed photoacoustic images (35 dB log gray scale dynamic range, 14 mm laterally by 40 mm axially) of a phantom with four point targets using (a) DAS, (b) DAS+MV, (c) DAS+CF, and (d) DAS+CF+MV.

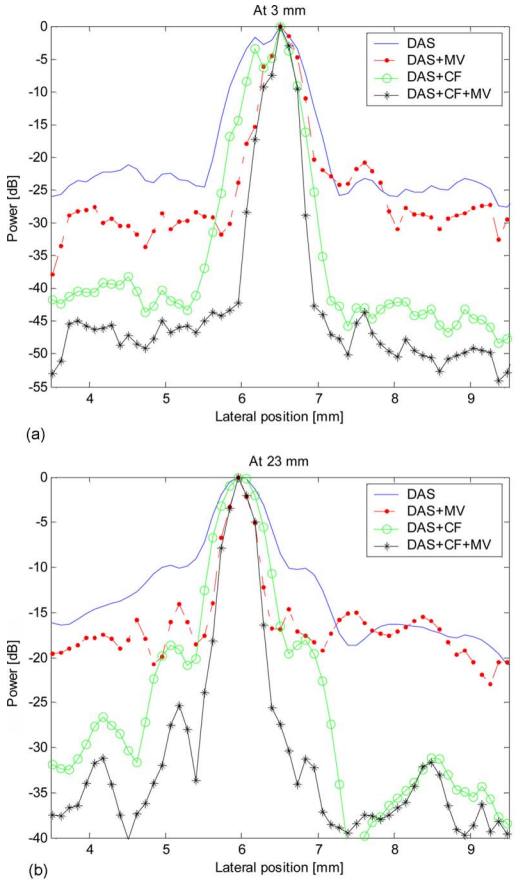

Fig. 2. (Color online) Lateral profiles of the PSF at (a) 3 and (b) 23 mm depths.

duces the sidelobes by 15–20 dB compared to simple DAS beamforming. Using the MV method with CF weighting, the sidelobe level is additionally lowered compared to the PSF using only CF weighting. Also, the width of the mainlobe in the CF weighted image was decreased approximately 20% to 30% from that of the simple DAS image. It was further reduced, by more than 20%, in the image reconstructed by combining the MV method and CF weighting.

Figure 3 shows the reconstructed photoacoustic images from the inclusion phantom, which used DAS beamforming with CF weighting and the MV method. The beamformed images, measuring 20 mm laterally by 20 mm axially, are displayed using a 45 dB log-scale dynamic range. Image contrast was calculated using the signal amplitude measured inside the inclusion and in the background [11]. The contrast of the beamformed images using DAS [Fig. 3(a)] is 15.92 dB, using DAS with the MV method [Fig. 3(b)] is 16.53 dB, using DAS with CF weighting [Fig. 3(c)] is 23.96 dB, and using DAS with the MV method and CF weighting [Fig. 3(d)] is 25.61 dB. As demonstrated in Fig. 3, the photoacoustic image using CF weighting was noticeably improved owing to the reduction of the sidelobe level since CF weighting retains the in-phase signal and reduces the out-of-phase signal. Although the improvement of the image quality using both MV and CF is subtle compared to CF weighting, the beamforming artifacts are still clearly reduced around the inclusion.

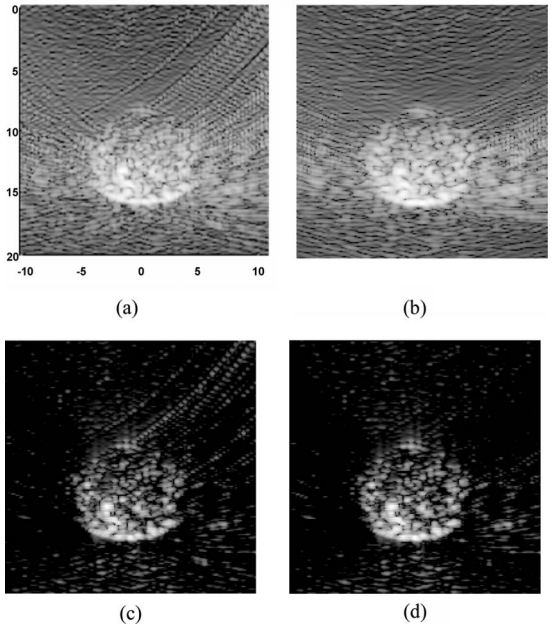

Fig. 3. Reconstructed photoacoustic images (45 dB dynamic range, 20 mm laterally by 20 mm axially) of a reconstructed phantom with a circular inclusion using (a) DAS, (b) DAS+MV, (c) DAS+CF, and (d) DAS+CF+MV.

In summary, the MV adaptive method and CF weighting were applied with DAS beamforming for photoacoustic imaging. Although CF weighting can significantly improve the photoacoustic image quality, the MV adaptive method can further enhance the spatial resolution and contrast. Experimental photoacoustic imaging studies demonstrated the superior performance of the MV adaptive method when combined with CF weighting.

Support in part by the National Institutes of Health under grants EB004963, EB008101, and HL091609 is gratefully acknowledged.

References

1. M. Xu and L. V. Wang, Rev. Sci. Instrum. **77**, 411011 (2006).
2. S. Park, S. R. Aglyamov, and S. Y. Emelianov, in *Proceedings of the 2007 IEEE Ultrasonics Symposium* (IEEE, 2007), pp. 856–859.
3. C. K. Liao, M. L. Li, and P. C. Li, Opt. Lett. **29**, 2506 (2004).
4. K. W. Hollman, K. W. Rigby, and M. O'Donnell, in *Proceedings of the 1999 IEEE Ultrasonics Symposium* (IEEE, 1999), pp. 1257–1260.
5. K. E. Thomenius, in *Proceedings of the 1996 IEEE Ultrasonics Symposium* (IEEE, 1996), pp. 1615–1622.
6. S. Park, S. Mallidi, A. B. Karpiouk, S. Aglyamov, and S. Y. Emelianov, Proc. SPIE **6437**, 141 (2007).
7. M. Sasso and C. C. Bacrie, in *Proceedings of the 2005 IEEE International Conference on Acoustics, Speech, and Signal Processing* (IEEE, 2005), pp. 489–492.
8. J. Capon, Proc. IEEE **57**, 1408 (1969).
9. J. F. Synnevag, A. Austeng, and S. Holm, IEEE Trans. Ultrason. Ferroelectr. Freq. Control **54**, 1606 (2007).
10. G. Mitic, K. J. J. Otto, E. Plies, G. Solkner, and W. Zinth, Appl. Opt. **33**, 6699 (1994).
11. J. L. Prince and J. M. Links, *Medical Imaging Signals and Systems* (Prentice Hall, 2006).